ACS APPLIED MATERIALS & INTERFACES

Letter

www.acsami.org

High-Performance Photoconductivity and Electrical Transport of ZnO/ZnS Core/Shell Nanowires for Multifunctional Nanodevice Applications

Sehee Jeong,[†] Minhyeok Choe,[‡,§] Jang-Won Kang,[‡] Min Woo Kim,[‡] Wan Gil Jung,[‡] Young-Chul Leem,[‡] Jaeyi Chun,[†] Bong-Joong Kim,[‡] and Seong-Ju Park*[,†,‡]

[†]Department of Nanobio Materials and Electronics and [‡]School of Materials Science and Engineering, Gwangju Institute of Science and Technology, Gwangju 500-712, Republic of Korea

Supporting Information

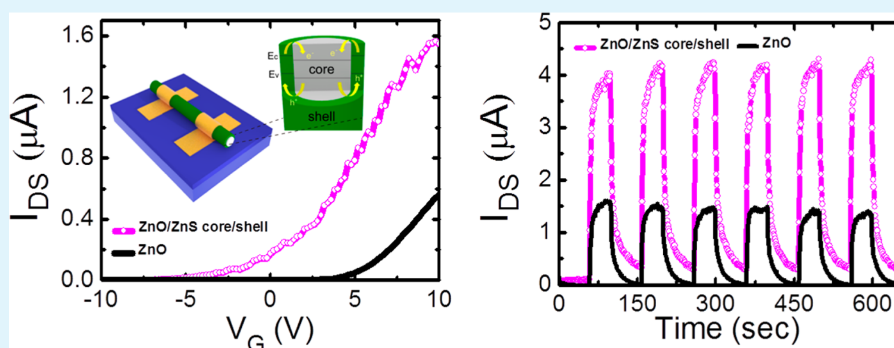

ABSTRACT: We report the electrical and optical properties of ZnO/ZnS core/shell nanowire (NW) devices. The spatial separation of charge carriers due to their type II band structure together with passivation effect on ZnO/ZnS core/shell NWs not only enhanced their charge carrier transport characteristics by confining the electrons and reducing surface states in the ZnO channel but also increased the photocurrent under ultraviolet (UV) illumination by reducing the recombination probability of the photogenerated charge carriers. Here the efficacy of the type-II band structure and the passivation effect are demonstrated by showing the enhanced subthreshold swing (150 mV/decade) and mobility (17.2 $cm^2/(V\ s)$) of the electrical properties, as well as the high responsivity (4.4×10^6 A/W) in the optical properties of the ZnO/ZnS core/shell NWs, compared with the subthreshold swing (464 mV/decade), mobility (8.9 $cm^2/(V\ s)$) and responsivity (2.5×10^6 A/W) of ZnO NWs.

KEYWORDS: *ZnO nanowire, ZnO/ZnS core/shell, type II band structure, passivation*

INTRODUCTION

One-dimensional semiconductor nanostructures have potential for realizing downscaled field-effect transistors (FETs), light-emitting diodes (LEDs), and laser diodes (LDs) for next-generation systems such as highly integrated memory chips and high-resolution displays.[1−6] In addition, their structural feature of a high surface-to-volume ratio is promising for the generation of highly sensitive photodetectors.[7−9] Among numerous candidates that can be used to manipulate the one-dimensional nanostructure system, ZnO nanowires (NWs) have been intensively investigated because of their attractive intrinsic properties such as their wide direct band gap (3.4 eV), large exciton binding energy (60 meV), chemical stability and piezoelectric properties.[10−12] The bandgap of ZnO NW can easily be adjusted by creating an alloy with other elements, and the simple synthesis of ZnO NWs with a novel band structure is available using chemical reactions.[13,14] The bandgap of a one-dimensional semiconductor is a critical parameter in determining the basic performance of a device, such as the electrical transport properties and optical responsivity. In case of ZnO/ZnS core/shell NWs, the valence and conduction bands of the core material are lower than those of the shell material. Thus, it provides a spatial separation of the electrons and holes in the core and shell caused by its type-II band structure.[14] As the shell layer is synthesized or deposited, the density of the surface states in ZnO NW systems can be efficiently managed for high-quality devices because the number of defects that cause degradation of the electrical and optical characteristics can be reduced.[15−17] A $Mg_{0.2}Zn_{0.8}O$ shell layer was reported to enhance the electrical properties of a ZnO-based FET and a ZnO/ZnS core/shell NW system was introduced to improve the performance of dye-sensitized solar cells.[18,19] Therefore, we expect that the type II band structure of ZnO/ZnS core/shell NWs, together with the passivation effect will enhance the critical parameters, such as the charge transport and response properties, leading to an improved performance of the FETs

Received: February 3, 2014
Accepted: April 14, 2014
Published: April 14, 2014

 © 2014 American Chemical Society

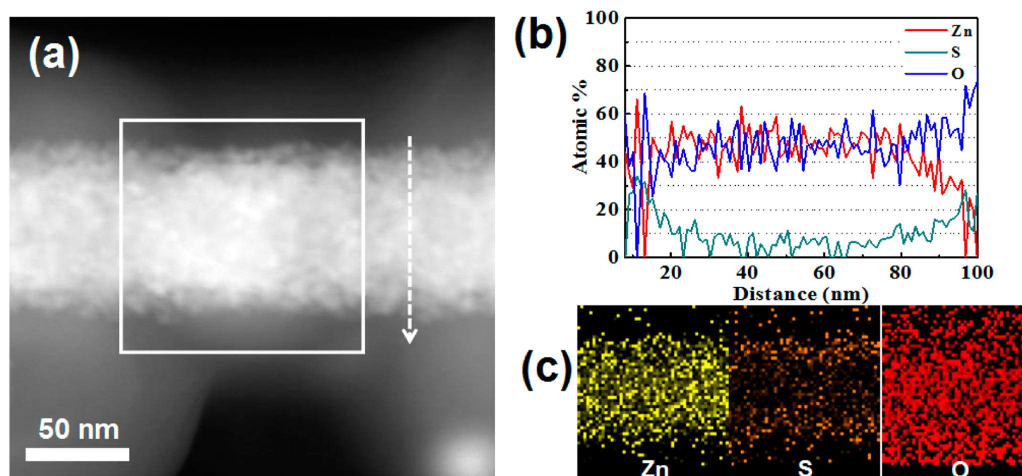

Figure 1. (a) HAADF STEM image of ZnO/ZnS core/shell NW. (b) EDX line scan for Zn, S, and O following the arrow in panel a. (c) EDX composition maps for Zn (left), S (middle), and O (right) of the boxed region in panel a.

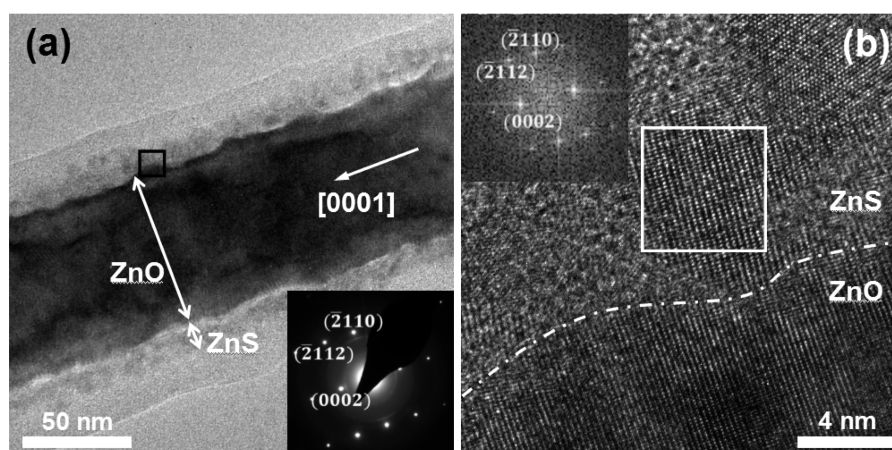

Figure 2. (a) Low-magnification bright-field TEM image of ZnO/ZnS core/shell NW. The inset is the SAED pattern of the core/shell NW. (b) High-resolution TEM image of the boxed region in panel a. The inset is the FFT image of the representative regions of the boxed regions in the shell.

and photodetectors. Until now, there have not been any reports on the electrical properties of high speed switching ZnO/ZnS core/shell NW FETs with optical properties that have a high sensitivity for use as a multifunctional nanodevice. Here the electrical and optical properties of ZnO/ZnS core/shell NW devices are studied to investigate the possibility of realizing high performance multifunctional nanodevices. The electrical properties of the ZnO/ZnS core/shell NWs were evaluated by studying single NW FETs, and the optical properties were investigated by illuminating the same FETs with ultraviolet (UV) light. We demonstrate the efficacy of the type II band structure and the passivation effect by measuring the enhanced subthreshold swing, mobility in the electrical properties as well as the fast responsivity in the optical properties and comparing them with ZnO NWs.

MATERIALS AND METHODS

1. Synthesis of ZnO/ZnS Core/Shell Nanowires. The ZnO NWs were grown by thermal chemical vapor deposition (CVD) through a vapor-phase transport process using a mixture of ZnO and graphite powder through the carbothermal reduction process.[20] We carried out the growth of ZnO NWs on 3 nm-thick Au-deposited sapphire substrates at 950 °C for 20 min under a constant gas flow of argon (100 sccm) and oxygen (2 sccm). We used the Au as a catalyst for the growth but we could not find any Zn−Au alloy or Au on top of the ZnO NWs by transmission electron microscopy (TEM) analysis (see Figure S1 in the Supporting Information), meaning that the growth mechanism of our ZnO NWs does not follow the traditional VLS mode.[20] To prepare the ZnO/ZnS core/shell NWs, the ZnO NW samples were then immersed in sodium sulfide (Na_2S) and zinc nitrate ($(Zn(NO_3)_2)$) solutions, both with a concentration of 0.16 mol/L, to deposit the ZnS shell layer at 60 °C for 2 h. This method for ZnO/ZnS core/shell NWs is also known as a well-known self-assembling method.[14,21] Even though the fabrications of one-dimensional ZnO/ZnS core/shell nanostructure have been achieved by using various methods including chemical vapor deposition, thermal sulfidation, and ion exchange in vapor, these methods require vacuum or high-temperature processes. However, the low-temperature solution method in this study is a very simple and facile method for low-cost production of NWs with high yield.[14,21,22]

To investigate the structure of ZnO/ZnS core/shell NWs, we carried out the energy-dispersive X-ray spectroscopy (EDX) line scan (Figure 1b) of the region as indicated by an arrow

mark in Figure 1a and compositional mapping (Figure 1c) of the boxed area in Figure 1a to acquire the elemental information on Zn, S, and O from high angle annular dark field scanning transmission electron microscopy (HAADF STEM) imaging (Figure 1a). These data indicate that the ZnS shell layer is deposited on the ZnO core NWs. However, it is not clear whether ZnS shell layer is oxidized so we performed TEM analysis on the ZnO/ZnS core/shell NWs.

Figure 2a shows a low-magnification bright-field transmission electron microscopy (BF TEM) image of a representative ZnO/ZnS core/shell NW with an inset for the selected area electron diffraction (SAED) pattern of this NW. These data indicate that the ZnO core NW is single crystalline and it is grown into [0001], whereas the ZnS shell is poly crystalline. The SAED pattern shows strong diffraction spots of single crystalline ZnO core and weak ring patterns of polycrystalline ZnS shell as shown in inset of Figure 2a. The structural information on the ZnO core NW is confirmed by a BF TEM image before depositing the ZnS shell, and the corresponding SAED pattern is shown in the Supporting Information, Figure S1. The structural properties of the ZnO/ZnS core/shell NW are also confirmed by the high-resolution TEM (HRTEM) image presented in Figure 2b. The HRTEM image was taken at $[01\bar{1}0]$ from the boxed region near the interface of the core/shell NW as shown in Figure 2a. We selected a region of the shell as indicated by a box in Figure 2b and the corresponding FFT pattern indicates that the region in the shell is single crystalline with a wurtzite (hexagonal) structure. This demonstrates that the shell is composed of ZnS rather than a compound material composed of Zn, S, and O because a compound material composed of Zn, S, and O elements is $ZnSO_4$ whose crystalline structure is normally orthorhombic (cubic) structure.[23]

We also carried out X-ray diffraction (XRD) analysis to further confirm the coating of ZnS layer on ZnO NWs. As shown in Figure 3, XRD spectrum of the ZnO/ZnS core/shell NWs was taken and compared to that of ZnO NWs. The both XRD patterns of the ZnO and ZnO/ZnS core/shell NWs show a predominant diffraction peak of ZnO at 34.5°, indicating the (002) diffraction peak of wurtzite ZnO. A new peak appears at 28.75°, which corresponds to (002) planes of wurtize structure of ZnS in the core/shell NWs.[21] The Au (111) peak has been also detected at 38.1° in both samples because we used Au catalyst.[24] Even though Au is not found on top of the ZnO NWs, the Au peak could be observed on XRD spectrum because Au films still remain between the NWs on the sapphire substrate.

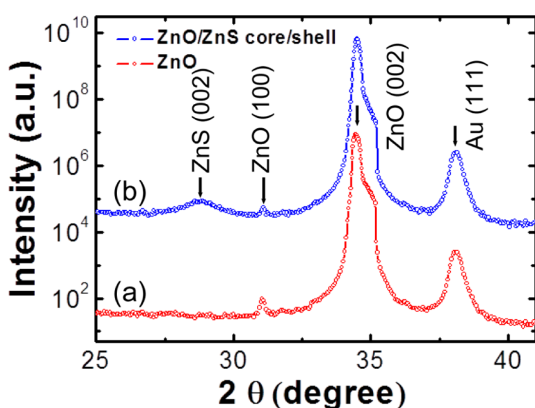

Figure 3. XRD patterns of (a) ZnO and (b) ZnO/ZnS core/shell NWs on sapphire substrates.

After synthesis of the ZnO/ZnS core/shell NWs, a rapid thermal annealing (RTA) process was carried out under various conditions to make smooth surfaces on the ZnS shells because the morphology of the ZnO/ZnS core/shell NWs was rough, as shown in Figure 1a. The surface morphology was improved by using the optimized annealing temperature of 700 °C for 5 min (see Figure S2 in the Supporting Information).

2. Fabrication Process of Devices Based on ZnO/ZnS Core/Shell and ZnO Nanowires. The ZnO/ZnS core/shell NWs were released by sonication in isopropyl alcohol (IPA), and then dispersed on a highly doped p-type silicon wafer with a 100 nm-thick SiO_2 layer. Standard photolithography was used to pattern the source and drain electrode.[25,26] The silver layer was used as an ohmic contact to ZnS shell layer in the ZnO/ZnS core/shell NWs,[27] and then Ti/Au was deposited. The thickness of Ag, Ti, and Au film was 5, 30, and 50 nm, respectively. The Ti/Au was deposited as an ohmic contact of ZnO NWs. Panels a and b in Figure 4 show a schematic diagram and a scanning electron microscope (SEM) image of a device. ZnO NW FETs were also prepared using the same fabrication and annealing method for the ZnO/ZnS core/shell NW FETs and were used as the reference sample.

3. Measurements of the Electrical and Optical Properties. The electrical properties of the ZnO/ZnS core/shell and ZnO NW FETs were systematically characterized using a semiconductor parameter analyzer (Agilent B1500A) at room temperature. The photoresponse of both types of NWs were examined using a portable UV lamp with an emission wavelength of 365 nm under an optical power density of 0.5 mW/cm^2. A Karl Suss 1000 UV intensity meter was used to calibrate the optical power density.

RESULTS AND DISCUSSION

Figure 5a shows representative output (I_{DS}–V_{DS}, source–drain current versus source-drain voltage) curves of the ZnO/ZnS core/shell and ZnO NW FETs with a gate voltage from −2 to 8 V, increasing in 2 V increments. The cumulatively increasing I_{DS} with an increasing gate voltage (V_G) indicates that both NWs are typically n-type semiconductors.

Figure 5b shows the representative transfer (I_{DS}–V_G, source–drain current versus gate voltage) curves for the ZnO/ZnS core/shell and ZnO NW FETs at a drain voltage of 5 V. The threshold voltage (V_{th}) of the ZnO/ZnS core/shell NW FETs is relatively shifted in the negative direction compared with that of the ZnO NW FETs. This result can be explained by the surface passivation because the reduced surface trap density in the ZnO and ZnS interface layer decreases the depletion region in the ZnO channel.[28] Confined electrons, resulting from the carrier separation of the type II band structure, could also contribute to the V_{th} shift toward the negative direction in the ZnO/ZnS core/shell NW FETs. As shown in Figure 5b, the V_{th} of the ZnO NW FETs distinctively exhibits enhancement-mode behavior, which indicates that a large number of surface states and deep traps exist in the channel or at the interface of the ZnO NWs.[29] The subthreshold swing (SS) is a critical parameter for the fast switching of FETs, and the SS of the ZnO/ZnS core/shell NW FETs is steeper than the ZnO NW FETs, as shown in the inset of Figure 5b. The SS for the ZnO/ZnS core/shell NW FETs is estimated to be 150 mV/decade and this value is significantly improved from the SS of 464 mV/decade for a ZnO NW FET. A faster transition between the off-

dx.doi.org/10.1021/am500731n | ACS Appl. Mater. Interfaces 2014, 6, 6170−6176

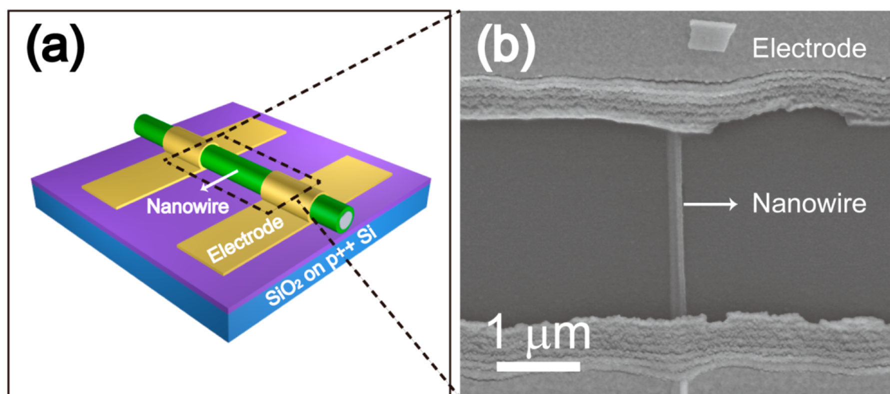

Figure 4. (a) Schematic illustration of a NW FET and (b) SEM image of the area selected in panel a.

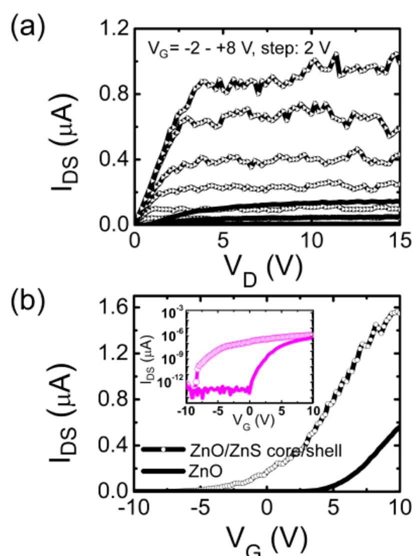

Figure 5. (a) I_{DS}−V_{DS} characteristics of ZnO/ZnS core/shell (triangular dot) and ZnO (solid line) NW FETs. V_G was swept from −2 V to +8 V in 2 V steps. (b) I_{DS}−V_G characteristics of ZnO/ZnS core/shell (circular dot) and ZnO (solid line) NW FETs. The inset indicates the log scaled I_{DS}−V_G curves of a ZnO/ZnS core/shell (circular dot) and ZnO (solid line) NW FETs.

to-on current of ZnO/ZnS core/shell NW FET, as shown in the inset of Figure 5b, is attributed to the reduced surface and interface states since the SS is proportional to the sum of the depletion capacitance (C_d) in the channel and the capacitance (C_{it}) of the surface and interface states.[18] To investigate the electron transport properties for both types of NW FETs, we estimated the electron mobility (μ) and concentration (n) using the cylinder on a conducting plate model as follows[28,30]

$$\frac{C_g}{L} = \frac{2\pi\varepsilon_{ox}\varepsilon}{\cosh^{-1}\left(1 + \frac{d}{r}\right)} \quad (1)$$

$$\mu_n = \frac{dI_{DS}}{dV_G}\frac{L^2}{V_{DS}C_g} \quad (2)$$

$$n_e = \frac{C_g|V_g - V_{th}|}{e\pi r^2 L} \quad (3)$$

where C_g is a gate capacitance, L is the channel length (~ 3 μm), r is the radius of the NWs, d is the thickness of the gate oxide layer (100 nm), ε is the dielectric constant (3.9 for SiO_2), dI_{DS}/dV_G is the transconductance (g_m), and V_{DS} is the source-drain voltage (5 V). The calculated electron mobility and charge carrier concentration of the ZnO/ZnS core/shell NW FETs are 17.2 $cm^2/(V\ s)$ and 2.1×10^{18} cm^{-3}, whereas those for the ZnO NW FETs are 8.9 $cm^2/(V\ s)$ and 6.1×10^{17} cm^{-3}, respectively. These results indicate that the enhanced mobility originates from the reduced density of surface trap states by passivating the ZnS shell layer, as well as the distribution of charge carriers, resulting from the transport mechanism for the type II band structure. In addition, the separation and confinement of the charge carriers are verified by the high concentration of electrons in the ZnO/ZnS core/shell NW FETs. Other ZnO/ZnS core/shell NW FETs have also exhibited similar behavior in their electrical characteristics (see Figure S3 in the Supporting Information).

The photoconductance and photoresponse properties of the ZnO/ZnS core/shell and ZnO NWs were measured under UV illumination, which was switched on-and-off in 40 and 60 s intervals. Note that a V_{DS} of 5 V was applied to the devices without a V_G for these measurements. Panels a and b in Figure 6 show the time dependent photocurrents for the ZnO/ZnS

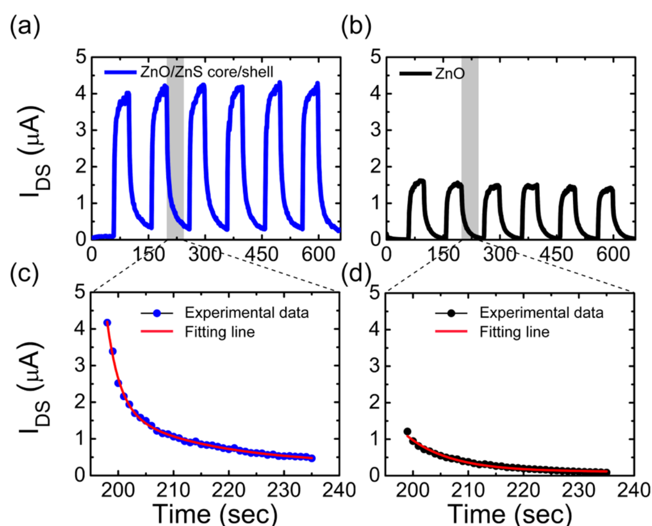

Figure 6. Time-dependent photoresponse currents of (a) ZnO/ZnS core/shell and (b) ZnO NW devices upon repeated UV illumination (365 nm) at a V_{DS} of 5 V. The extracted time dependent photoresponse current (circular dot) and their fitting curves (solid line) for (c) ZnO/ZnS core/shell and (d) ZnO NWs.

core/shell and ZnO NW devices. After turning on the UV light, both photocurrents immediately increased from the off state to the on state and their responses from the periodical UV switching were consistently reproduced. The ZnO/ZnS core/shell NWs showed a higher photocurrent by 176% compared with that of the ZnO NWs, indicating that a high photoresponsivity can be obtained from the ZnO/ZnS core/shell NWs. In general, the responsivity and external quantum efficiency are key parameters in determining the sensitivity of optoelectronic devices.[31] The responsivity (R) is defined as $R = \Delta I/PS$, which is the generated photocurrent per unit power of the incident light on the effective area of a photoconductor. ΔI is the difference between the photocurrent and the dark current, P is the density of light power irradiated on the NW and S is the irradiated area of an individual NW.[32] The calculated responsivity of the ZnO/ZnS core/shell NW (4.4×10^6 A/W) was much higher than that of the ZnO NW (2.5×10^6 A/W) due to the large difference between the photocurrent and dark current in the ZnO/ZnS core/shell NW by the type II band structure. This result can be ascribed that the recombination probability of the photogenerated electron and hole pairs decreases in ZnO/ZnS core/shell NW because of the spatial separation of charge carriers, resulting from the type II band structure. In addition, rough surface of ZnO/ZnS core/shell NWs may also contribute partly to the high photocurrent because ZnS shell shows a rough surface which may enhance light absorption of core NWs. The external quantum efficiency (EQE) can be expressed as $\text{EQE} = (hc/e\lambda)R$, where R is responsivity, h is Planck's constant, c is the velocity of the light, e is the charge of an electron and λ is the wavelength of the irradiated light, which is related to the number of electron−hole pairs excited by one absorbed photon.[32] The EQEs calculated for the ZnO/ZnS core/shell and ZnO NWs are 1.5×10^9% and 8.5×10^8%, respectively. It is believed that the remarkably high responsivity and external quantum efficiency of the ZnO/ZnS core/shell NWs originate from the spatial separation and confinement of the photogenerated electrons and holes upon illumination, resulting from the type II band alignment. We fabricated 14 devices of ZnO/ZnS core/shell and ZnO NWs and obtained consistent results showing that responsivity and external quantum efficiency are much improved in ZnO/ZnS core/shell NWs devices (see Figure S4 in the Supporting Information).

Panels c and d in Figure 6 show an expanded view of the time-dependent photocurrents shown in panels a and b in Figure 6 (gray region) and their fitting curves, respectively. The decay of photocurrents were fitted with a biexponential decay equation: $I = I_0 + A\exp(-(t/\tau_1)) + B\exp(-(t/\tau_2))$, where τ_1 and τ_2 are fast and slow decay times.[33,34] Here, the fast decay time of 2.3 s for the ZnO/ZnS core/shell NW is much shorter than that of 8.1 s for the ZnO NW. We also compared the rise times of ZnO/ZnS core/shell NWs by fitting the data as shown in Figure S5 in the Supporting Information. The initial rise times are 2.5 and 3.1 s for ZnO/ZnS core/shell and ZnO NWs, respectively. Even though the rise times of ZnO/ZnS core/shell is slightly faster than ZnO NWs, the photoresponse current of ZnO/ZnS core/shell NWs is about two times higher than ZnO NWs when the UV light is turned on. These results indicate that ZnO/ZnS core/shell NWs have a potential with outstanding performance for high speed switching of photo sensing devices compared to ZnO NWs.

We also calculated the photocurrent to dark current ratio of ZnO and ZnO/ZnS core/shell NWs. Figure 7 presents current

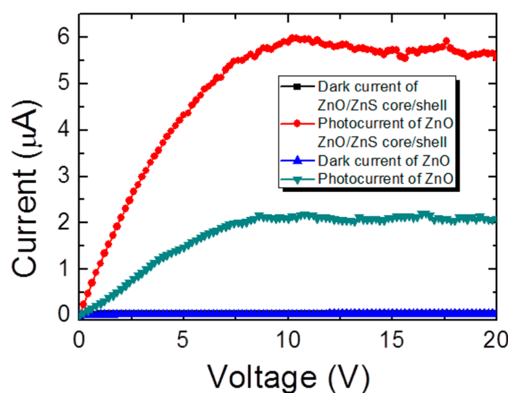

Figure 7. Current to voltage ($I-V$) plot of the ZnO/ZnS core/shell and ZnO NWs showing the dark current and photocurrent under UV light of 365 nm.

to voltage ($I-V$) characteristics of ZnO/ZnS core/shell and ZnO NWs in the dark and photocurrent under illumination of UV light with a 365 nm wavelength.[35] The dark current and photocurrent of the ZnO/ZnS core/shell NWs are at 3.81×10^{-8} A and 4.32×10^{-6} A at a bias voltage of 5 V, respectively, whereas ZnO NWs show a dark current of 3.00×10^{-8} A and a photocurrent of 1.47×10^{-6} A. Therefore, the photocurrent to dark current ratio of ZnO/ZnS core/shell and ZnO NWs are 113 and 49, respectively. Even though dark current of ZnO/ZnS core/shell NWs are higher than ZnO NWs presumable due to the lattice mismatch and defect, the photocurrent to dark current ratio is much higher than ZnO NWs due to its high photocurrent.[36] Therefore, ZnO/ZnS core/shell NWs have a high photo to dark current ratio with high responsivity, which is a significant advantage for the high-performance photodetectors with type II band structure.

The enhanced electrical and optical properties of the ZnO/ZnS core/shell NWs can be explained by energy-band diagrams. Panels a and b in Figure 8 show energy-band diagrams of the cross-sectional regions in the ZnO and ZnO/ZnS core/shell NW devices, respectively. For the ZnO NWs, the electrons trapped in the surface states or defects can

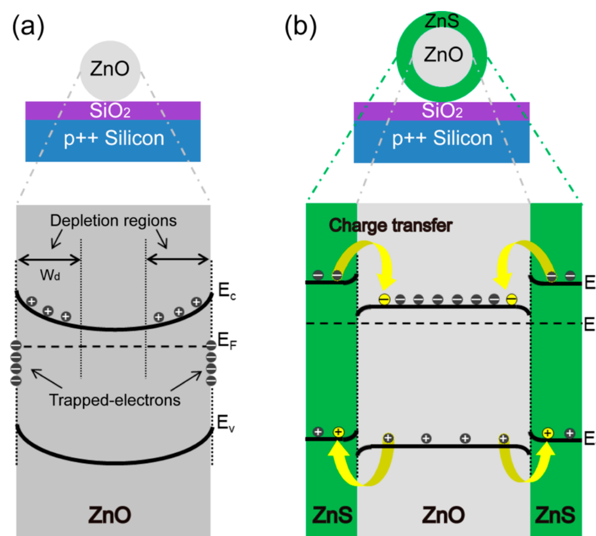

Figure 8. Schematic illustration of the cross-sectional views and their corresponding energy band diagrams of (a) a ZnO and (b) a ZnO/ZnS core/shell NW device.

generate a depletion region in the ZnO channel by band bending (Figure 8a), resulting in the disturbance of the charge carrier transport.[28] However, the ZnS shell layer reduces the surface states in ZnO NWs by the passivation effect, diminishing the depletion region and enhancing the charge carrier transport. Even though there are many interfacial traps at the grain boundaries resulting from polycrystalline structure and surface states in the ZnS shell, the charge transport through the ZnO core would be enhanced by reduced surface state of ZnO. In addition, the potential energy gradient at the interface between ZnO and ZnS separates and confines the electrons and holes in the conduction band (E_c) of the ZnO and in the valence band (E_v) of the ZnS, respectively (Figure 8b). We believe that this ideal distribution of charge carriers, where the electrons are in the ZnO channel and the holes are in the ZnS shell of the ZnO/ZnS core/shell NW FETs, contributes to the improvement of the charge transport properties. Therefore, these two synergetic effects increase the conductivity (σ) of the ZnO/ZnS core/shell NW FETs on the basis of the Drude model where $\sigma = ne\mu$. Furthermore, the spatial separation of the carriers also reduces the recombination probability of the photogenerated electron and hole pairs. Therefore, the photocurrent of the ZnO/ZnS core/shell NWs is significantly increased compared with that of the ZnO NWs, under illumination of UV light. This is mainly responsible for high responsivity and external quantum efficiency of the ZnO/ZnS core/shell NW nanodevices. It is expected that the type II band structure, along with the passivation effect has the potential to achieve a high performance in multifunctional nanodevices.

CONCLUSIONS

Coating a ZnS shell on ZnO NWs reduced the surface states and induced charge carrier confinement by the type-II band structure. The FETs based on ZnO/ZnS core/shell NWs showed a small SS of 150 mV/decade and a high mobility of 17.2 $cm^2/(V\ s)$, as well as a high responsivity of 4.4×10^6 A/W and a fast switching time upon UV illumination switching. The enhancement of the electrical and optical properties of the ZnO/ZnS core/shell nanodevices compared with ZnO NWs is attributed to the spatial separation and confinement of the charge carriers because of the type-II band structure, together with the passivation effect. It is expected that the ZnO/ZnS core/shell NWs provide versatility to realize multifunctional nanoscaled electronic and optoelectronic devices with fast switching speeds and high photosensitivity for the next-generation electronic devices.

ASSOCIATED CONTENT

Supporting Information

TEM images of ZnO and ZnO/ZnS core/shell NW, and electronic and photoresponse properties of ZnO/ZnS core/shell NWs and ZnO NWs. This material is available free of charge via the Internet at http://pubs.acs.org.

AUTHOR INFORMATION

Corresponding Author

*E-mail: sjpark@gist.ac.kr.

Present Address

[§]M.C. is currently at System LSI Division, Samsung Electronics, Yongin-City, Republic of Korea

Notes

The authors declare no competing financial interest.

ACKNOWLEDGMENTS

This research was supported by the National Research Foundation of Korea (NRF) grant funded by the Korea government (MSIP) (2008-0062606, CELA-NCRC). B.J.K. acknowledges the support from the support from the National Research Foundation of Korea (NRF) grant funded by the Korea government (2013R1A1A1007978).

REFERENCES

(1) Lieber, C. M.; Wang, Z. L. Functional Nanowires. *MRS Bull.* **2007**, *32*, 99−108.

(2) Duan, X.; Huang, Y.; Cui, Y.; Wang, J.; Lieber, C. M. Indium Phosphide Nanowires as Building Blocks for Nanoscale Electronc and Optoelectronic devices. *Nature* **2001**, *409*, 66−69.

(3) Cui, Y.; Lieber, C. M. Functional Nanoscale Electronic Devices Assembled Using Silicon Nanowire Building Blocks. *Science* **2001**, *291*, 851−853.

(4) Huang, M. H.; Mao, S.; Feick, H.; Yan, H.; Wu, Y.; Kind, H.; Weber, E.; Russo, R.; Yang, P. Room-Temperature Ultraviolet Nanowire Nanolasers. *Science* **2001**, *292*, 1897−1899.

(5) Huang, Y.; Duan, X.; Cui, Y.; Lauhon, L. J.; Kim, K.-H.; Lieber, C. M. Logic Gates and Computation from Assembled Nanowire Building Blocks. *Science* **2001**, *294*, 1313−1317.

(6) Bao, J.; Zimmler, M. A.; Capasso, F.; Wang, X.; Ren, Z. F. Broadband ZnO Single-Nanowire Light-Emitting Diode. *Nano Lett.* **2006**, *6*, 1719−1722.

(7) Kind, H.; Yan, H.; Messer, B.; Law, M.; Yang, P. Nanowire Ultraviolet Photodetectors and Optical Switches. *Adv. Mater.* **2002**, *14*, 158−160.

(8) Chen, G.; Liu, Z.; Liang, B.; Yu, G.; Xie, Z.; Huang, H.; Liu, B.; Wang, X.; Chen, D.; Zhu, M.-Q.; Shen, G. Single-Crystalline p-Type Zn_3As_2 Nanowires for Field-Effect Transistors and Visible-Light Photodetectors on Rigid and Flexible Substrates. *Adv. Funct. Mater.* **2013**, *23*, 2681−2690.

(9) Hu, L.; Yan, J.; Liao, M.; Xiang, H.; Gong, X.; Zhang, L.; Fang, X. An Optimized Ultraviolet-A Light Photodetector with Wide-Range Photoresponse Based on ZnS/ZnO Biaxial Nanobelt. *Adv. Mater.* **2012**, *24*, 2305−2309.

(10) Schrier, J.; Demchenko, D. O.; Wang, L. W.; Alivisatos, A. P. Optical Properties of ZnO/ZnS and ZnO/ZnTe Heterostructures for Photovoltaic Applications. *Nano Lett.* **2007**, *7*, 2377−2382.

(11) Yang, P.; Yan, H.; Mao, S.; Russo, R.; Johnson, J.; Saykally, R.; Morris, N.; Pham, J.; He, R.; Choi, H. J. Controlled Growth of ZnO Nanowires and Their Optical Properties. *Adv. Funct. Mater.* **2002**, *12*, 323−331.

(12) Wang, Z. L.; Song, J. H. Piezoelectric Nanogenerators Based on Zinc Oxide Nanowire Arrays. *Science* **2006**, *312*, 242−246.

(13) Hsu, H. C.; Wu, C. Y.; Cheng, H. M.; Hsieh, W. F. Band Gap Engineering and Stimulated Emission of ZnMgO Nanowires. *Appl. Phys. Lett.* **2006**, *89*, 013101.

(14) Meng, X. Q.; Peng, H.; Gai, Y. Q.; Li, J. Influence of ZnS and MgO Shell on the Photoluminescence Properties of ZnO Core/Shell Nanowires. *J. Phys. Chem. C* **2009**, *114*, 1467−1471.

(15) Tajik, N.; Chia, A. C. E.; LaPierre, R. R. Improved Conductivity and Long-term Stability of Sulfur-Passivated n-GaAs Nanowires. *Appl. Phys. Lett.* **2012**, *100*, 203122.

(16) Song, S.; Hong, W.-K.; Kwon, S.-S.; Lee, T. Passivation Effects on ZnO Nanowire Field Effect Transistors under Oxygen, Ambient, and Vacuum Environments. *Appl. Phys. Lett.* **2008**, *92*, 263109.

(17) Jones, F.; Leonard, F.; Talin, A. A.; Bell, N. S. Electrical Conduction and Photoluminescence Properties of Solution-Grown ZnO Nanowires. *J. Appl. Phys.* **2007**, *102*, 014305.

(18) Lee, C.-H.; Yoo, J.; Doh, Y.-J.; Yi, G.-C. $ZnO/Mg_{0.2}Zn_{0.8}O$ Coaxial Nanorod Heterostructures for High-performance Electronic Nanodevice Applications. *Appl. Phys. Lett.* **2009**, *94*, 043504.

(19) Chung, J.; Myoung, J.; Oh, J.; Lim, S. Synthesis of a ZnS Shell on the ZnO Nanowire and Its Effect on the Nanowire-Based Dye-Sensitized Solar Cells. *J. Phys. Chem. C* **2010**, *114*, 21360−21365.

(20) Geng, C.; Jiang, Y.; Yao, Y.; Meng, X.; Zapien, J. A.; Lee, C. S.; Lifshitz, Y.; Lee, S. T. Well-Aligned ZnO Nanowire Arrays Fabricated on Silicon Substrates. *Adv. Funct. Mater.* **2004**, *14*, 589−594.
(21) Li, J.; Zhao, D.; Meng, X.; Zhang, Z.; Zhang, J.; Shen, D.; Lu, Y.; Fan, X. Enhanced Ultraviolet Emission from ZnS-Coated ZnO Nanowires Fabricated by Self-Assembling Method. *J. Phys. Chem. B* **2006**, *110*, 14685−14687.
(22) Hu, Y.; Qian, H.; Liu, Yu.; Du, G.; Zhang, F.; Wang, L.; Hu, X. A Microwave-assisted Rapid Route to Synthesize ZnO/ZnS core-shell Nanostructures via Controllable Surface Sulfidation of ZnO Nanorods. *CrystEngComm* **2011**, *13*, 3438−3443.
(23) Wildner, M.; Giester, M. G. Crystal structure refinements of synthetic chalcocyanite ($CUSO_4$) and zincosite ($ZnSO_4$). *Mineral. Petrol* **1988**, *39*, 201−209.
(24) Huang, M. H.; Wu, Y.; Feick, H.; Tran, N.; Weber, E.; Yang, P. Catalytic Growth of Zinc Oxide Nanowires by Vapor Transport. *Adv. Mater.* **2001**, *13*, 113−116.
(25) Hong, W.-K.; Jo, G.; Sohn, J. I.; Park, W.; Choe, M.; Wang, G.; Kahng, Y. H.; Welland, M. E.; Lee, T. Tuning of the Electronic Characteristics of ZnO Nanowire Field Effect Transistors by Proton Irradiation. *ACS Nano* **2010**, *4*, 811−818.
(26) Choe, M.; Park, W.; Kang, J.-W.; Jeong, S.; Hong, W.-K.; Lee, B. H.; Park, S.-J.; Lee, T. Investigation of Threshold Voltage Instability Induced by Gate Bias Stress in ZnO Nanowire Field Effect Transistors. *Nanotechnology* **2012**, *23*, 485201.
(27) Borah, J. P.; Sarma, K. C. Optical and Optoelectronic Properties of ZnS Nanostructured Thin Film. *Act Phys. Polonica, A* **2008**, *114*, 713−719.
(28) Hong, W.-K.; Sohn, J. I.; Hwang, D. K.; Kwon, S.-S.; Jo, G.; Song, S.; Kim, S. M.; Ko, H. J.; Park, S.-J.; Welland, M. E.; Lee, T. Tunable Electronic Transport Characteristics of Surface-Architecture-Controlled ZnO Nanowire Field Effect Transistors. *Nano Lett.* **2008**, *8*, 950−956.
(29) Dehuff, N. L.; Kettenring, E. S.; Hong, D.; Chiang, H. Q.; Wager, J. F.; Hoffman, R. L.; Park, C. H.; Keszler, D. A. Transparent Thin-Film Transistors With Zinc Indium Oxide Channel Layer. *J. Appl. Phys.* **2005**, *97*, 064505.
(30) Lind, E.; Persson, A. I.; Samuelson, L.; Wernersson, L. E. Improved Subthreshold Slope in an InAs Nanowire Heterostructure Field-Effect Transistor. *Nano Lett.* **2006**, *6*, 1842−1846.
(31) Konstantatos, G.; Sargent, E. H. Nanostructured Materials for Photon Detection. *Nat. Nanotechnol.* **2010**, *5*, 391−400.
(32) Li, L.; Wu, P.; Fang, X.; Zhai, T.; Dai, L.; Liao, M.; Koide, Y.; Wang, H.; Bando, Y.; Golberg, D. Single-Crystalline CdS Nanobelts for Excellent Field-Emitters and Ultrahigh Quantum-Efficiency Photodetectors. *Adv. Mater.* **2010**, *22*, 3161−3165.
(33) Cheng, G.; Wu, X.; Liu, B.; Li, B.; Zhang, X.; Du, Z. ZnO Nanowire Schottky Barrier Ultraviolet Photodetector with High Sensitivity and Fast Recovery Speed. *Appl. Phys. Lett.* **2011**, *99*, 203105.
(34) Bera, A.; Basak, D. Photoluminescence and Photoconductivity of ZnS-Coated ZnO Nanowires. *ACS Appl. Mater. Interfaces* **2010**, *2*, 408−412.
(35) Afsal, M.; Wang, C. Y.; Chu, L. W.; Ouyang, H.; Chen, L. J. Highly Sensitive Metal-Insulator-Semiconductor UV Photodetectors Based On ZnO/SiO_2 Core-Shell Nanowires. *J. Mater. Chem.* **2012**, *22*, 8420−8425.
(36) Chang, S. J.; Liu, C. W.; Hsiao, C. H.; Lo, K. Y.; Young, S. J.; Kao, T. H.; Tsai, K. S.; Wu, S. L. Noise Properties of Fe-ZnO Nanorod Ultraviolet Photodetectors. *IEEE Photonics Technol. Lett.* **2013**, *25*, 2089−2092.